Computers and Electronics in Agriculture 127 (2016) 625–632

Contents lists available at ScienceDirect

Computers and Electronics in Agriculture

journal homepage: www.elsevier.com/locate/compag

Original papers

Temporal dynamics of maize plant growth, water use, and leaf water content using automated high throughput RGB and hyperspectral imaging

Yufeng Ge [a,*], Geng Bai [a], Vincent Stoerger [b], James C. Schnable [b,c]

[a] Department of Biological Systems Engineering, University of Nebraska-Lincoln, Lincoln, NE 68583, USA
[b] Center for Plant Science Innovation, University of Nebraska-Lincoln, Lincoln, NE 68588, USA
[c] Department of Agronomy & Horticulture, University of Nebraska-Lincoln, Lincoln, NE 68583, USA

ARTICLE INFO

Article history:
Received 28 January 2016
Received in revised form 6 July 2016
Accepted 23 July 2016
Available online 29 July 2016

Keywords:
Drought
High throughput phenotyping
Hyperspectral
Image processing
RGB
Water use efficiency

ABSTRACT

Automated collection of large scale plant phenotype datasets using high throughput imaging systems has the potential to alleviate current bottlenecks in data-driven plant breeding and crop improvement. In this study, we demonstrate the characterization of temporal dynamics of plant growth and water use, and leaf water content of two maize genotypes under two different water treatments. RGB (Red Green Blue) images are processed to estimate projected plant area, which are correlated with destructively measured plant shoot fresh weight (FW), dry weight (DW) and leaf area. Estimated plant FW and DW, along with pot weights, are used to derive daily plant water consumption and water use efficiency (WUE) of the individual plants. Hyperspectral images of plants are processed to extract plant leaf reflectance and correlate with leaf water content (LWC). Strong correlations are found between projected plant area and all three destructively measured plant parameters ($R^2 > 0.95$) at early growth stages. The correlations become weaker at later growth stages due to the large difference in plant structure between the two maize genotypes. Daily water consumption (or evapotranspiration) is largely determined by water treatment, whereas WUE (or biomass accumulation per unit of water used) is clearly determined by genotype, indicating a strong genetic control of WUE. LWC is successfully predicted with the hyperspectral images for both genotypes ($R^2 = 0.81$ and 0.92). Hyperspectral imaging can be a very powerful tool to phenotype biochemical traits of the whole maize plants, complementing RGB for plant morphological trait analysis.

1. Introduction

One of the greatest challenges facing modern agriculture is to produce enough food and energy for a world population likely to reach 9.7 billion by 2050. In the past several decades, the yields of major food crops have increased substantially as a result of increased inorganic fertilizer use, improved agronomic practices, and genetic improvement. However, the current rate of increase in yield will not keep pace with this increased demand for food and fuel over the next 35 years (Grassini et al., 2013). Plant phenomics, the use of holistic large scale approaches to collect plant phenotypic information, has the potential to spark a new green revolution. It would fill the gap between the low cost of generating large scale datasets of plant genotypes and the time consuming and expensive process of collecting large scale plant phenotypic datasets. Advancement in plant phenomics would enable more effective utilization of genetic data, and ultimately lead to novel gene discovery and improved crop yield and quality in the field.

Phenotypic data collected from plants grown in the field is arguably the most informative for guiding plant breeding efforts (Furbank and Tester, 2011). However, field based phenotyping strategies face two major challenges. First, high quality plant phenotypic data is difficult to obtain in natural field conditions. For examples, wind will make plant images blurred and unsuitable for quantitative analysis; and fast fluctuating radiation levels (due to presence of clouds, for example) significantly reduce the accuracy of passive type spectroscopic measurements. Second, field grown plants exhibit greater variability as a result of uncontrollable environmental conditions (such as spatial and temporal variations in solar radiation, soil property, microclimate and pest pressure). This increased variability renders the detection and quantification of genetic factors influencing phenotype more

* Corresponding author at: Department of Biological Systems Engineering, 209 Chase Hall, East Campus, University of Nebraska-Lincoln, Lincoln, NE 68583, USA.
E-mail address: yge2@unl.edu (Y. Ge).

http://dx.doi.org/10.1016/j.compag.2016.07.028
0168-1699/

challenging. These challenges can be effectively addressed in controlled-environment phenotyping facilities. The two major components of the variability that can be largely decoupled from genetic factors influencing plant phenotypes are (1) the phenotypic variation caused by the intrinsic inhomogeneity of soil/aerial environment, and (2) the instrument response variation caused by the temporal and spatial variations of radiation, temperature, and humidity. Therefore, plant phenotyping in controlled environments, while not as effective for predicting the performance of commercial plant varieties under field conditions, can be particularly useful in studying how plant phenotypes vary among differing genotypes in response to controlled stress conditions, as well as how interactions between genetic and environmental factors can produce unanticipated phenotypic responses.

High throughput plant phenomics studies in controlled environments (growth chambers and greenhouses) emerge in the literature about ten years ago. Early studies involve small scale experiments that use custom developed systems (in terms of imaging hardware and software) and focus on model plant *Arabidopsis thaliana* (Granier et al., 2006; Jansen et al., 2009). The imaging modules commonly employed are RGB (Red Green Blue; Golzarian et al., 2011), steady state fluorescence and pulse amplitude modulated fluorescence (Jansen et al., 2009; Konishi et al., 2009), and thermal infrared (Jones et al., 2009; Romano et al., 2011). Recently, investment in capital-intensive high throughput phenotyping greenhouses has started to enable larger scale studies which involve hundreds of plants with continuous imaging of weeks to months (Chen et al., 2014; Yang et al., 2014; Fahlgren et al., 2015; Neilson et al., 2015; Campbell et al., 2015). High throughput plant phenotyping has really become a highly integrative inter-disciplinary field that attracts not only plant scientists but also engineers (Li et al., 2014; Kim and Glenn, 2015; Sankaran et al., 2015; Mangus et al., 2016).

Humplík et al. (2015) conducted a review of automated phenotyping of plant shoots for analysis of plant stress responses using large scale phenomics platforms. RGB, fluorescence, NIR and thermal IR imaging systems have all appeared in the literature, with RGB by far the most frequently used imaging module. It is clear from this review article that wheat, barley and rice are the most studied crops. Although maize is a very important staple crop around the world, there appears to be a lack of information in maize regarding high throughput phenotyping studies (in particular at the public sector), possibly as a result of the large stature of even pre-reproductive stage maize plants. This study focuses on maize. Our specific objective is to use a high throughput plant imaging/phenotyping facility to characterize the temporal dynamics of plant shoot growth and water use, and plant leaf water content of two maize genotypes under two water treatments.

2. Materials and methods

2.1. High throughput imaging greenhouse and experiment design

The experiment was conducted in the LemnaTec 3D Scanalyzer system (LemnaTec GmbH, Aachen, Germany) at University of Nebraska-Lincoln. The system consists of four imaging chambers. Table 1 below summarizes the imaging modules and their key parameters in these chambers. The chambers are designed to permit the imaging of plants up to a nominal height of 2.5 m, allowing the phenotyping of crop species such as maize and some energy sorghum varieties through reproductive stage (Supplemental Fig. 1). The system also incorporates an automated weighing and watering station where the change in pot weight as a result of water evaporation and transpiration can be quantified, and prescribed amounts of water can be precisely applied.

Table 1
The four chambers and imaging modules of the LemnaTec 3D Scanalyzer system in this study.

Imaging chamber	Camera maker	Position	Key parameters
Visible (RGB)	Basler	Side, Top	Image size: 2454 × 2056 pixel
Thermal infrared	Basler	Side, Top	Measured emission wavelength: 8–14 μm Image size: 480 × 640 pixel
Steady state fluorescence	Basler	Side, Top	Excitation wavelength: 400–500 nm Measured emission wavelength: 500–750 nm Image size: 1038 × 1390 pixel
Hyperspectral	Headwall	Side	Wavelength range: 550–1750 nm Spectral bandwidth: 5 nm Imaging detector pixel number: 320 Image formation: vertical scanning

Two maize inbred genotypes, B73 and FFMM-A (Fast Flowering Mini Maize-A) (40 plants each, 80 plants total), were used in this study. B73 is a public sector, stiff stalk heterotic group inbred which was widely used as a female parent in hybrid corn production, and is broadly employed in maize genetic research today. FFMM-A is a rapid cycling variety developed through the intercrossing of conventional early flowering maize varieties with flint and popcorn lines. FFMM-A reaches a stature of 0.7–0.9 m and flowers approximately 30 days after planting. B73 is therefore a typical representative of the temperate inbred lines used to produce the vast majority of hybrid corn in the US, while FFMM-A represents one extreme end of the total morphological variation present in the species (with the other end consisting of tropical maize genotypes which can grow to 4–4.5 m and never flower when grown in the American corn belt).

After the seeds were sown, the pots were kept off the system's conveyor belt and hand watered to soil saturation for plant establishment. On six Days after Sowing (DAS 6), the pots were transferred to the conveyor belt and daily acquisition of plant images and automated water application began. To minimize the effect of the temporal variation of maize physiology (within a day) on measurement, imaging was scheduled to begin at 10 AM and end at 12 PM every day. Individual plants received one of two water treatments (control versus drought). In the control group, a target pot weight of 5400 g was maintained throughout the experiment. In the drought group, the pots were first maintained at 5400 g until DAS 10. After that, no water was added to those pots, causing a progressive drought stress to the plants till the end of the experiment.

The greenhouse temperature was regulated between 18 and 25 °C. The pots used are roughly 22 cm in diameter and 20 cm in height, with a capacity of 5.68 L. The pot substrate was made by mixing Fafard germination soil, water, Osmocote Plus 15-9-12 (fertilizer), and Micromax micronutrients at predetermined ratio. The estimated volumetric water content of soil for the control group (maintain 5400 g of pot weight by adding water daily) was 25% and was approximately 85% of field capacity. This was to ensure ample water supply in the control group while not too wet to cause root respiration inhibition. The bottom of the pots is sealed meaning that no water can be lost through percolation, which allows the calculation of water loss through evapotranspiration with water mass balance.

The experiment was conducted at two stages. The first stage was from DAS 6 to 26 when all 80 plants were placed on the conveyor belt, automatically watered/weighed at the station, and imaged daily. At five time points (DAS 13, 16, 20, 24, and 26) one plant from each of the four genotype-treatment combinations

was destructively sampled (a total of 20). For each plant, all plant material above soil was harvested and weighed immediately to obtain shoot fresh weight (FW), and then fractionated to leaves and stem. Leaf Area (LA) was measured with a leaf area meter (LI-3100C Area Meter, LI-COR Biosciences, Lincoln, NE). The plant material was then placed in an oven at 70 °C for 24 h for shoot dry weight (DW). Plant leaf water content (LWC) was derived as $\frac{FW_{leaf}-DW_{leaf}}{FW_{leaf}} \times 100\%$, where FW_{leaf} and DW_{leaf} are fresh weight and dry weight of the leaf fraction, respectively. Destructive measurements are later used to establish correlation with image-based phenotypes.

At the second stage (DAS 26 to 46), the remaining 60 (80-20) plants were moved off the conveyor belt and allowed to continue to grow in the same greenhouse. For the control group, ~120 g of water was manually applied to each pot daily; and for the drought group, no water was applied. Imaging and destructive sampling were conducted at four times during this stage (DAS 32, 34, 39 and 46). At each time point, four or eight plants (one or two from each category) were manually loaded onto the conveyor belt for imaging. These plants were then destructively sampled following the same protocol as in the first stage to measure FW, LA, DW, and LWC. A total of 24 plants were destructively sampled at Stage Two. A workflow diagram of the experiment is provided in Supplemental Fig. 2.

The focus of the first stage of the experiment was to derive (1) LA, shoot FW and DW accumulation curves of maize plants, and (2) daily water consumption and water use efficiency, for both genotypes under both water treatments. As the experiment progressed into the second stage, plants were undergoing severe drought stress. This significantly lowered LWC and created a large range in LWC. Therefore, the focus of the second stage of the experiment was to investigate the usefulness of hyperspectral imaging to predict LWC.

2.2. RGB and hyperspectral image analysis and spectral modeling

Plant images were first exported from the LemnaTec database using the LemnaBase software. While there are plant phenotyping image processing software (such as PlantCV reported in Fahlgren et al., 2015; ImageHarvest in Campbell et al., 2015; and LemnaGrid), our study included hyperspectral images that none of these image processing software packages currently have the ability to process. We used MATLAB (version 2015b, MathWork®, Natick, MA) with its Image Processing Toolbox to develop algorithms and process plant images. The major task of image processing was to extract plant pixels from RGB (two side views and one top view) and hyperspectral images from which image-based plant phenotypes can be derived. RGB images were transformed to single band images use the index $2 \times G/(B+R)$; where R, G, and B are the Red, Green, and Blue components. This index emphasizes the green component in RGB pixels, and minimizes the effect of non-consistent illumination among different images (Meyer and Neto, 2008). A threshold value of 1.15 was determined to effectively segment plant pixels from background. Morphological opening was then used (with a 3-by-3 square structural element) to remove isolated noises. The total pixel count of the plant from both zero to 90 degree side views were then averaged as plant Projected Area (PA, or equivalently, pixel count). All maize plants were consistently oriented in the pot carriers to ensure the maximum unobstructed plant images taken at zero degree side view and to avoid any bias in PA among maize plants. PA is used to establish the correlation with destructively measured shoot FW, DW, and LA.

The top view image was excluded from calculations of plant PA. At later developmental stages, tall plants are much closer to the top view camera, making plants to appear larger, introducing significant bias in the calculation of plant PA.

The following procedures were used to process the hyperspectral images. First, images at Band 27 (670 nm) and Band 48 (770 nm) were used to calculate an NDVI (Normalized Difference Vegetation Index) image: $(Band48 - Band27)/(Band48 + Band27)$. Note that there are many combinations of a red and an NIR channel to generate NDVI; and here we chose the pair that is most commonly used (Muñoz-Huerta et al., 2013). The NDVI image can be used to effectively segment the plant from background by setting a threshold of 0.25. Second, the image at Band 131 (1160 nm), in which the plant leaves were consistently much brighter (higher pixel intensity) than the stem, was used with the NDVI image to further classify the plant into the stem and leaves. Pixels belonging to plant leaves were then used as a template to extract pixel intensity from all hyperspectral bands. This gave an average leaf reflectance spectrum for each plant (See Supplemental Fig. 3). Fig. 1 below summarizes the procedure for hyperspectral image analysis.

The extracted plant leaf reflectance spectra were used to predict LWC using partial least squares regression (PLSR). The size of the PLSR models (number of PLSR latent factors) was determined by selecting the number of latent factors giving the first local minimum in Root Mean Squared Error of Cross Validation ($RMSE_{CV}$). Statistics including R^2 (Coefficient of Determination), $MAPE_{CV}$ (Mean Absolute Percent Error of Cross Validation), and RPD (Ratio of Performance to Deviation, defined as Standard Deviation of the data divided by $RMSE_{CV}$) were also calculated for model assessment. PLSR modeling was performed in R statistical environment (R Core Team, 2015) with pls package (Mevik et al., 2013).

In this study, we focused on RGB and hyperspectral images, although images of four imaging modules were available (Table 1). Because of the configuration of the imaging routine, plants had to wait in the head house for some time before imaging. This forced plant leaf temperature and the photosynthetic processes quickly to be in equilibrium with the head house environment (which was significantly different from the greenhouse in terms of temperature and radiation intensity). This made the thermal IR imaging and the steady state fluorescence imaging module less effective to distinguish maize plants between the two water treatments.

2.3. Calculation of daily water consumption and water use efficiency

The automated watering and weighing station of the system, together with estimated shoot FW and DW, allows the estimation of daily water consumption (or equivalently, evapotranspiration, ET) and water use efficiency (WUE) of each plant. Consider two consecutive days i and $i+1$.

$$ET = [(W_{(i,after)} - FW_i) - (W_{(i+1,before)} - FW_{i+1})]/T \quad (1)$$

$$WUE = (DW_{i+1} - DW_i)/ET \quad (2)$$

where $W_{(i,\ after)}$ is the total pot weight after water application for Day i; $W_{(i+1,\ before)}$ is the total pot weight before water application for Day $i+1$; FW_i and FW_{i+1} is shoot fresh weight estimated at the point of imaging for Day i and $i+1$, respectively; and DW_i and DW_{i+1} is shoot dry weight estimated at the point of imaging for Day i and $i+1$, respectively. T is the time interval and is equal to 1 day (daily pot weighing following the same schedule every day).

A numerical example from our data on how daily ET and WUE were calculated is given below. The weight of a certain pot on DAS 17 was 5398 g after watering. The estimated shoot FW and DW were 17.53 and 1.53 g, respectively. On DAS 18, the pot weight before watering was 5304 g. The estimated shoot FW and DW were 24.13 and 2.21 g, respectively. Water consumption between DAS 17 and 18 was calculated as $[(5398 - 17.53) - (5304 - 24.13)] = 100.6$ g/day. There was also an accumulation of net shoot dry biomass of $2.21 - 1.53 = 0.68$ g/day. WUE was then calculated as

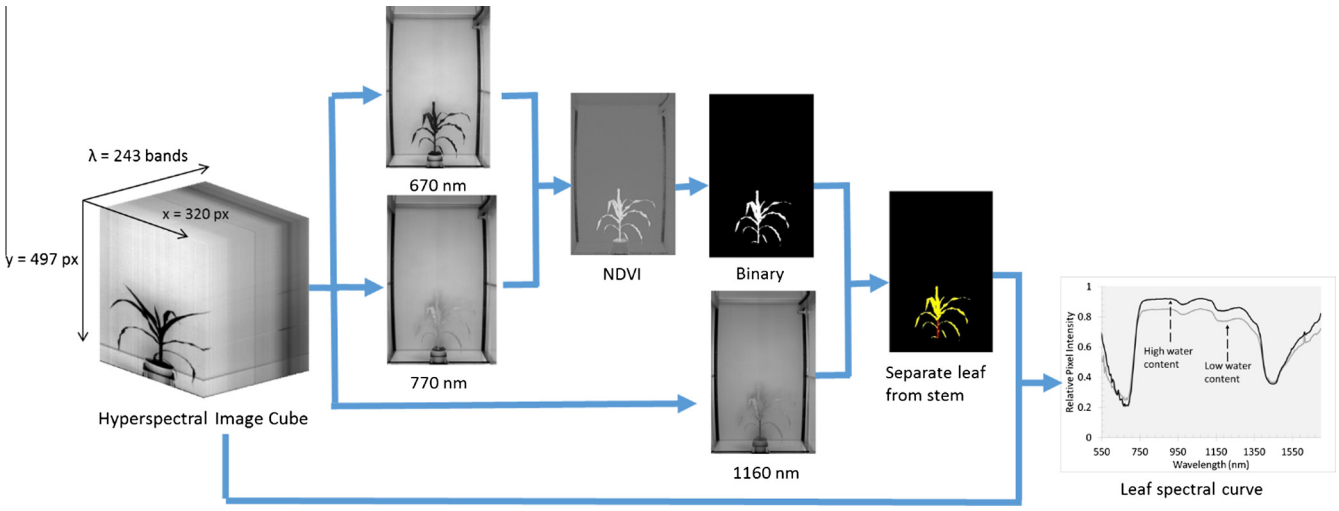

Fig. 1. Procedures of hyperspectral image analysis to extract leaf pixels and the average leaf reflectance (pixel intensity) information. Average leaf reflectance spectra were used to predict plant leaf water content.

0.68/100.6 = 0.0068 g/g (6.8 g of shoot dry matter per 1000 g of water consumption).

WUE is commonly defined as a ratio of biomass accumulation to water consumed. Depending on specific research goals, biomass accumulation can be defined as carbon assimilation, crop biomass, or grain yield; and water consumption can be transpiration, evapotranspiration, or total water input to the system. Here we define WUE as the amount of shoot dry matter produced per unit of water loss through evapotranspiration (Tuberrosa, 2012).

3. Results and discussion

3.1. Relationships between plant projected area and shoot fresh weight, dry weight, and leaf area for the maize plants

Fig. 2 shows the correlation between plant PA from two side view (0 and 90°) RGB images and destructively measured LA, shoot FW and DW for the first experimental stage (DAS 6 to 26). It can be seen that LA and shoot FW are highly linearly correlated with PA ($R^2 > 0.98$); whereas shoot DW is best modeled with a second order polynomial with a slightly lower R^2 (0.952). It is also evident that, at this stage, the B73 and FFMM-A genotypes can be modeled together. Although B73 and FFMM-A are different in their plant architecture, at this growth stage, the differences are quite small.

Fig. 3 shows the relationships between PA from two side view RGB images and destructively measured LA, shoot FW and DW combining the data from Stages 1 and 2. With the inclusion of data from Stage 2 greater scatter is observed in the relationship between image-derived PA and destructively measured biomass. In general, shoot FW and DW of FFMM-A appear to be estimated higher than B73, given the same level of plant projected area. This agrees with our expectation. During the second stage of the experiment, FFMM-A plants started to develop tillers (secondary branches) and appear bushier than B73 (See Supplemental Fig. 4). A greater portion of the plant material is therefore occluded and not viewed by the RGB camera. This would lead to an underestimate of shoot fresh and dry weight for FFMM-A. It should be noted that, genotype specific biases for the pixel count based method for biomass estimation, are also documented in other phenotyping studies (Golzarian et al., 2011).

Fig. 4 shows the accumulation of shoot FW of 60 maize plants by genotype and water treatment at the first stage of the experiment (DAS 6 to 26). The temporal dynamics of growth patterns can be clearly identified. From DAS 6 to DAS 10 when the drought stress had not started, the difference was mainly between genotypes, with B73 showing greater shoot FW than FFMM-A. DAS 11 to DAS 17 saw the onset of drought and the two water treatment groups started to separate in shoot FW (though not very large differences). From DAS 18 to DAS 26, the control group consistently showed significantly higher shoot FW than the drought group for both genotypes. Note that at approximately DAS 20/21, shoot FW of the FFMM-A plants in the control group exceeded that of the B73 plants in the drought group.

3.2. Daily water consumption and water use efficiency

Fig. 5A shows the daily water consumption of the maize plants as calculated by Eq. (1) for the first stage of the experiment (DAS 7 to 26). It can be seen that, from DAS 7 to DAS 14, there is no obvious difference in daily water consumption either by genotype or treatment. At this time period, the plants were all small and evaporative loss from pot surface accounted for the majority of water consumption. The day-to-day variation in water loss can therefore be attributed mainly to the variation in day-to-day greenhouse climate (such as radiation load and vapor pressure deficit, see Supplemental Fig. 5). From DAS 15 to DAS 26, the control group showed significantly higher daily water consumption than the drought group, likely as a combined result of increased water demand from larger control plants, as well as the initiation of water conserving drought stress responses (e.g. stomatal closure) in the drought treated plants.

Fig. 5B shows the daily WUE of the maize plants for the first stage of the experiment. WUE remained low for both species from DAS 7 to 15. This is because evaporative loss from the pot surface accounted for a large portion of ET and therefore low WUE. When the plants grew bigger, transpiration loss became more significant, which increased WUE. When comparing WUE to daily water consumption in Fig. 5A, it can be seen that, while daily water consumption is mainly influenced by water treatment, WUE is mainly determined by genotype. It is evident in Fig. 5B that B73 consistently shows a higher WUE than FFMM-A.

WUE is an important concept for irrigation and drought tolerance research, and is a target trait for many breeding programs (Condon et al., 2004). The estimation of WUE usually involves close monitoring of all water inputs and outputs of the system and destructive harvesting of crops. Traditional WUE, therefore, is cal-

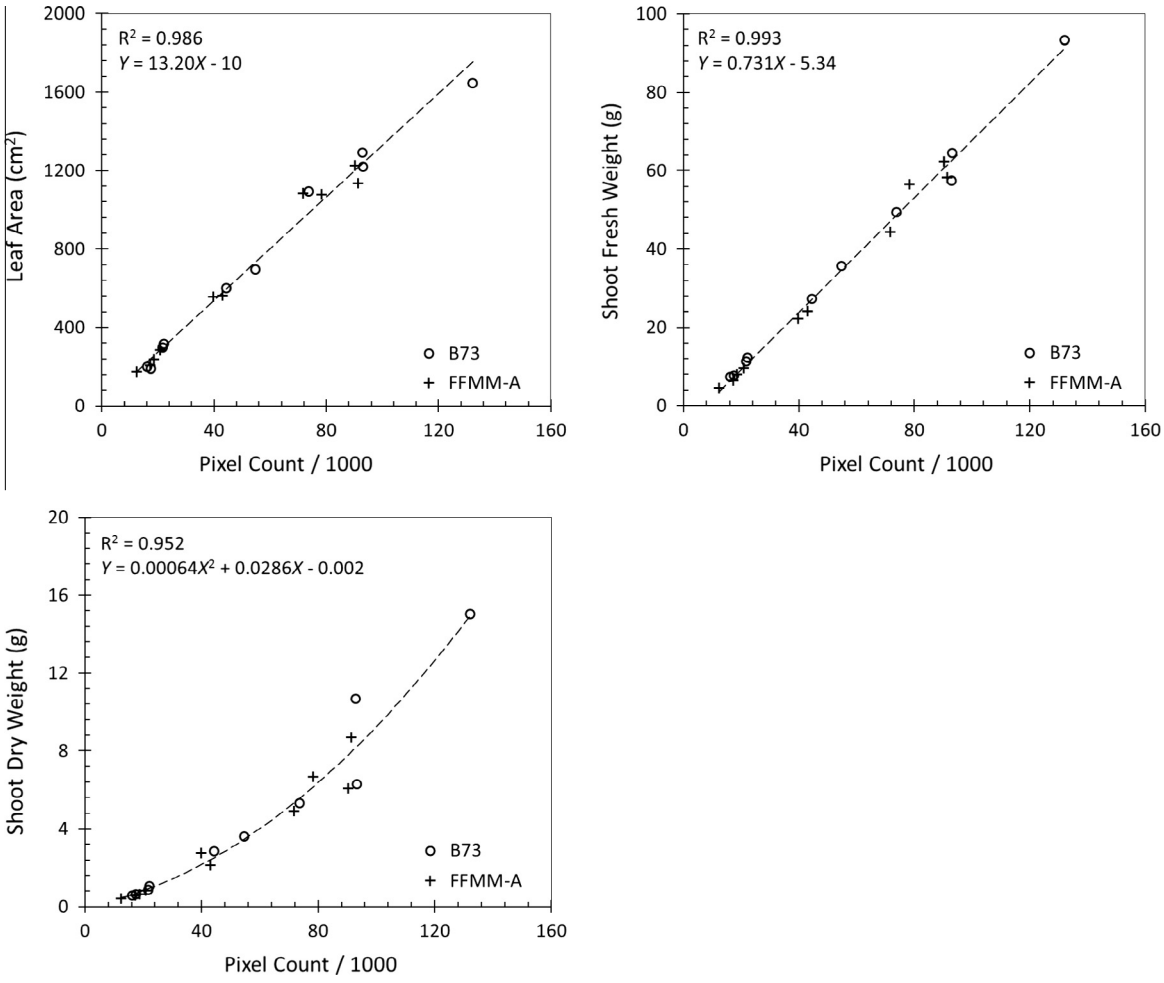

Fig. 2. Correlations between destructively measured leaf area, shoot fresh weight, shoot dry weight and plant projected area (pixel count) of maize plant RGB images for the first stage of the experiment (DAS 6 to 26). Circles represent individual destructively harvested B73 plants, and crosses represent individual FFMM-A plants. The total number of plants is 20.

culated on a seasonal basis when crops are mature and harvested. Here we demonstrate that, with nondestructive imaging (which allows estimation of plant shoot FW and DW) and automated pot weighing capability of the high throughput phenotyping facility, WUE of individual plants can be estimated on a daily basis. By grouping daily WUE, it is also possible to estimate WUE at particular growth stages along plant's life cycle. This would allow the better investigation of genetic basis of WUE, which may be controlled by different genetic factors at different stages of plant development, and upscale WUE of individual plants in the greenhouse to plant communities in the field.

3.3. Prediction of plant leaf water content from hyperspectral imaging

The range of LWC for all 44 destructively sampled plants (combining Stage 1 and 2) is from 68.1 to 92.3%, with a mean of 80.1% and a standard deviation of 8.5%. Images of four maize plants (one from each genotype and treatment group) on DAS 46 in Supplemental Fig. 6 provide a visual assessment of the severity of drought at the end of the experiment. Table 2 gives the results of predicting LWC with the reflectance spectra extracted from the plant hyperspectral images. Overall hyperspectral imaging can satisfactorily predict LWC for FFMM-A, B73, or the two genotypes combined. In the case of B73 (highest accuracy), the R^2 value is 0.92 and RPD equals 3.78. In chemometrics modeling, RPD is a widely used criterion for model evaluation (Fearn, 2002): RPD < 1.5 (poor model), 1.5 < RPD < 2.0 (useful model with potential improvement), 2.0 < RPD < 3.0 (good model), RPD > 3.0 (analytical quality). By this criterion, the models developed in Table 2 are "good" or "analytical quality" models, indicating the excellence of hyperspectral imaging for quantifying LWC. Fig. 6 is a scatterplot showing the correlation between measured versus predicted LWC for the two genotypes combined.

It can be seen that, when modeled separately, B73 gives better prediction accuracy than FFMM-A. This can be attributed to two reasons. First, at late stage of the experiment, FFMM-A plants appear to be bushier than B73 (Supplemental Fig. 4). A larger fraction of the plant leaves are occluded from the hyperspectral camera and the pixels extracted from the images are therefore less representative of the entire plants. Secondly, because of the rapid lifecycle of FFMM-A, this analysis includes plants developing reproductive organs (tassels and cobs). Compared to leaves, these organs have subtle differences in spectral signatures, which would lower the prediction accuracy.

Several studies have employed imaging systems to estimate LWC (Chen et al., 2014; Neilson et al., 2015). These studies used NIR cameras (spectral response 900–1700 nm) to capture a single NIR band. While it is proved possible to differentiate water treatments using pixel intensities extracted from the NIR images, quantitative determination of LWC from NIR images has not been demonstrated. Total NIR reflectance appears to be influenced by leaf thickness in addition to water content, introducing confound-

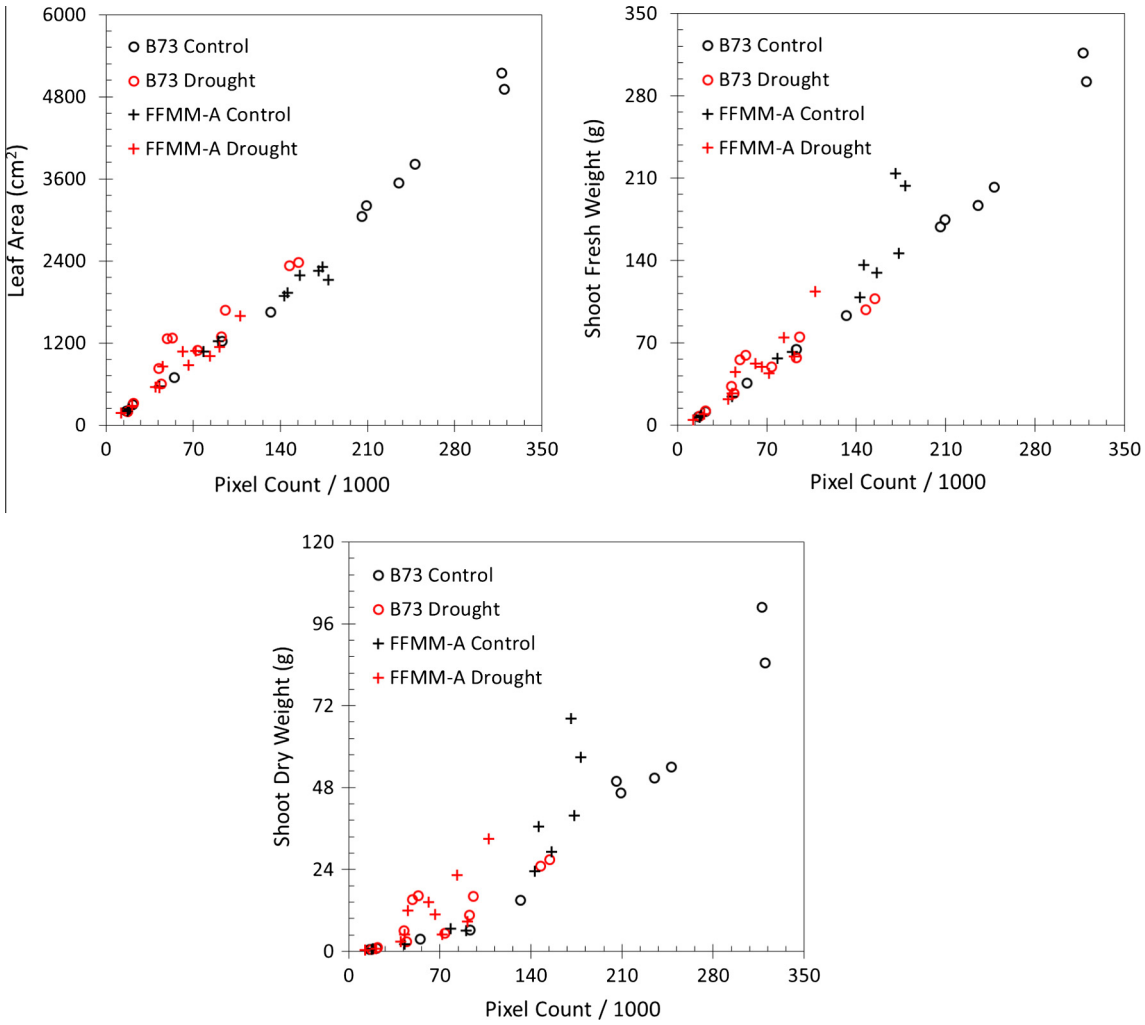

Fig. 3. Scatterplots showing the relationships between destructively measured leaf area, shoot fresh weight, shoot dry weight and plant projected area (pixel count) from maize plant RGB images combining the first and second stages of the experiment (DAS 6 to 46). Circles represent individual destructively harvested B73 plants, and crosses individual FFMM-A plants. Control plants are shown in black; and drought stressed plants are shown in red. The number of plants is 44.

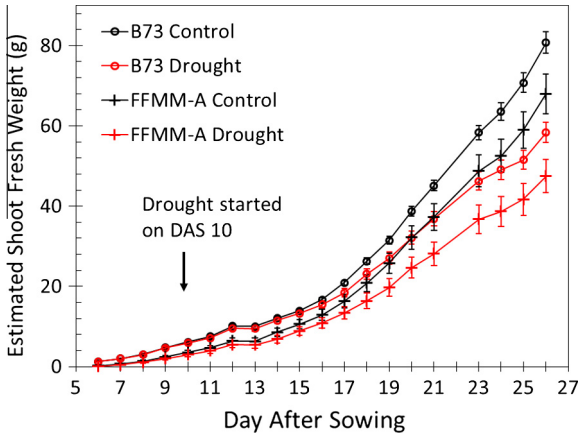

Fig. 4. Accumulation of shoot fresh weight of 60 maize plants at the first stage of the experiment (DAS 6 to 26). Each curve consists of data from the 15 plants which were not destructively harvested at any point in the first stage of the experiment. The error bar is the standard error of the mean for each group. Shoot fresh weight for each plant-day is estimated from the plant projected area of RGB image analysis using the linear regression developed in Fig. 2. Data points were missing on DAS 22 due to an unexpected disruption of the automated imaging routine on that day.

ing variation (Neilson et al., 2015). Here we show that hyperspectral imaging can predict LWC accurately (in case of B73, a prediction accuracy of ±2.3% is achieved as indicated by $RMSE_{CV}$). The advantages of hyperspectral imaging come from several aspects. First, using different image bands in the hyperspectral cube, plants can be more accurately segmented from the background and leaves can be accurately distinguished from stems (which is quite challenging with a RGB or NIR image). Second, hyperspectral images are capably of capturing the full spectral signature of plants, allowing more advanced analytical tools such as PLSR for modeling of leaf biochemical properties.

Hyperspectral imaging is used in a wide variety of agricultural and biological applications including remote sensing of crops (Blackburn, 2007) and food quality analysis and control (Gowen et al., 2007). Non-imaging spectroscopic analyses are also widely used to characterize the biochemical properties of grain and forage (Norris et al., 1976; Shenk et al., 2008). Based on these previous knowledges, hyperspectral imaging is suggested as a powerful tool in plant phenotyping to complement RGB analysis (to obtain plant chemical traits in addition to morphological traits). To the best of our knowledge, our study is the first to use a hyperspectral imaging system to measure leaf water content of whole living maize plants.

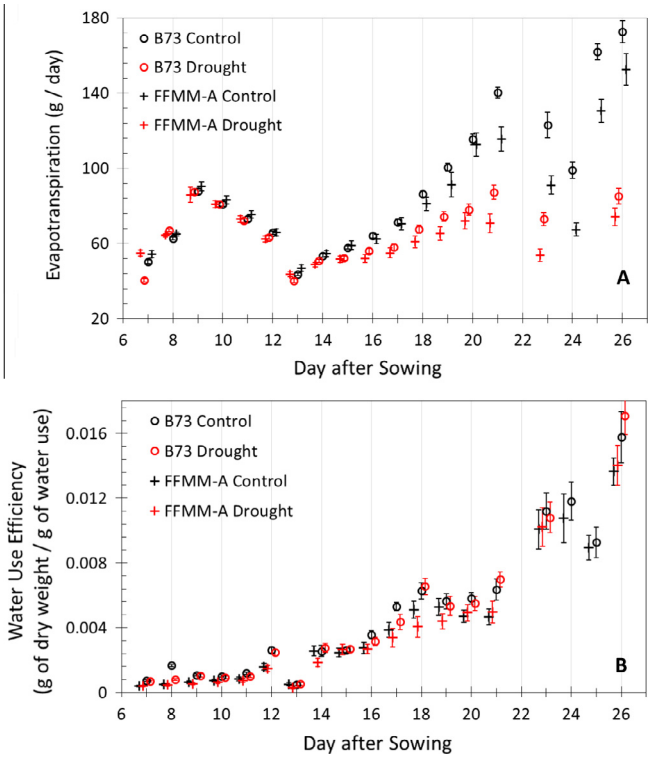

Fig. 5. Daily water consumption (or evapotranspiration) and water use efficiency of the 60 maize plants at the first stage of the experiment (DAS 6 to 26). Black indicates the control group and red indicates the drought group; circles indicate B73 and crosses indicate FFMM-A. The error bar is the standard error of the mean for each group. Data were missing on DAS 22 due to an unexpected disruption of the automated imaging routine on that day. Data for the drought treatment plants were also missing on DAS 24 and 25 due to an unexpected disruption of the automated watering station occurred.

Table 2
Results of predicting leaf water content from hyperspectral images of the maize plants.

Genotype	# of PLSR latent factors	$RMSE_{CV}$ (%)	$MAPE_{CV}$ (%)	R^2	RPD
FFMM-A (n = 22)	7	3.7	3.6	0.81	2.38
B73 (n = 22)	6	2.3	2.2	0.92	3.78
All (n = 44)	6	3.0	2.9	0.87	2.82

$RMSE_{CV}$ is Root Mean Squared Error of Cross Validation. $MAPE_{CV}$ is Mean Absolute Percent Error of Cross Validation. RPD is Ratio of Performance to Deviation (Standard Deviation of the dataset divided by $RMSE_{CV}$).

It is quite likely that this technique can be extended to quantify plant chemical phenotypes including nitrogen content, photopigment concentration, and mineral content.

4. Conclusion and future work

In this study, we used the high throughput imaging greenhouse at University of Nebraska-Lincoln to phenotype two maize genotypes (B73 and FFMM-A) in response to two levels of water application (control and drought). The focus was to use RGB images and automated pot weights to characterize temporal dynamics of maize plants' growth and water use, and hyperspectral imaging to quantify plant leaf water content. The major conclusions drawn from this study are:

1. Plant projected area extracted from two side views of maize RGB images can be accurately related to destructively measured plant shoot fresh weight, shoot dry weight, and leaf area at the early growth stage ($R^2 > 0.95$). However, such relationships become less strong for all parameters at the later growth stage when the difference in plant architecture of different genotypes becomes more evident.
2. Nondestructively estimated shoot fresh weight and dry weight (from images), together with automated pot weight measurements, allow the estimation of daily water consumption and water use efficiency for individual plants. While water consumption is determined in large by water treatment (in particular for the later growth stage when plant stature becomes large), water use efficiency is found to be determined by genotype.
3. Plant water content can be satisfactorily predicted with the reflectance spectra extracted from plant hyperspectral images. The prediction is more accurate for B73 than FFMM-A. This is due to the fact that, at the late growth stage, FFMM-A plants exhibit more complex plant structure and develop reproductive organs with different spectral signatures from plant leaves. Hyperspectral imaging can be a powerful tool to phenotype other important plant biochemical properties such as nitrogen, pigments, and trace minerals.

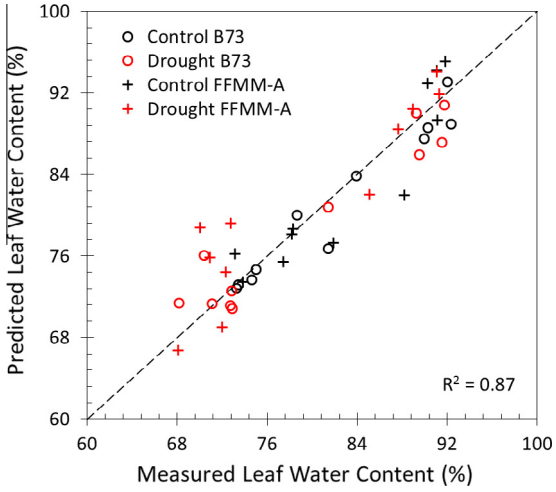

Fig. 6. Scatterplot of predicted versus measured plant leaf water content using the spectral information extracted from hyperspectral images of maize plants. This plot combines data from both B73 and FFMM-A. The dashed line is 1:1 line.

We suggest that future work include the following aspects. Firstly, more maize genotypes should be tested to elucidate any potential genotype effect on image-derived phenotypes from high throughput imaging. In our study, genotype has a clear effect on the calculation of side view projected area from RGB images, but does not show an effect on leaf water content estimation from hyperspectral images. Successful testing on more maize genotypes would allow us to draw a more solid conclusion on the usefulness of hyperspectral imaging, and extend the applicability of the hyperspectral models for leaf water content prediction. Second, new imaging protocols should be tested to minimize plants' waiting time in the head house before imaging. This would make the thermal IR and steady state fluorescence imaging useful for water-stress related plant phenotyping experiments.

Acknowledgements

Funds for this work was provided by Agricultural Research Division of the University of Nebraska-Lincoln.

Appendix A. Supplementary material

Supplementary data associated with this article can be found, in the online version, at http://dx.doi.org/10.1016/j.compag.2016.07.028.

References

Blackburn, G.A., 2007. Hyperspectral remote sensing of plant pigments. J. Exp. Bot. 58 (4), 855–867.

Campbell, M.T., Knecht, A.C., Berger, B., Brien, C.J., Wang, D., Walia, H., 2015. Integrating image-based phenomics and association analysis to dissect the genetic architecture of temporal salinity responses in rice. Plant Physiol. 168, 1476–1489.

Chen, D., Neumann, K., Friedel, S., Kilian, B., Chen, M., Altmann, T., Klukas, C., 2014. Dissecting the phenotypic components of crop plant growth and drought responses based on high-throughput image analysis. Plant Cell 26, 4636–4655.

Condon, A.G., Richards, R.A., Rebetzke, G.J., Farquhar, G.D., 2004. Breeding for high water-use efficiency. J. Exp. Bot. 55, 2447–2460.

Fahlgren, N., Feldman, M., Gehan, M., Wilson, M.S., Shyu, C., Bryant, D.W., Hill, S.T., McEntee, C.J., Warnasooriya, S.N., Kumar, I., Ficor, T., Turnipseed, S., Gilbert, K.B., Brutnell, T.P., Carrington, J.C., Mockler, T.C., Baxter, I., 2015. A versatile phenotyping system and analytics platform reveals diverse temporal responses to water availability in Setaria. Molecular Plant 8, 1–16.

Fearn, T., 2002. Assessing calibrations: SEP, RPD, RER and R^2. NIR News 13, 12–14.

Furbank, R.T., Tester, M., 2011. Phenomics – technologies to relieve the phenotyping bottleneck. Trends Plant Sci. 16 (12), 635–644.

Golzarian, M.R., Frick, R.A., Rajendran, K., Berger, B., Roy, S., Tester, M., Lun, D.S., 2011. Accurate inference of shoot biomass from high-throughput images of cereal plants. Plant Methods 7, 2.

Gowen, A.A., O'Donnell, C.P., Cullen, P.J., Frias, J.M., 2007. Hyperspectral imaging – an emerging process analytical tool for food quality and safety control. Trends Food Sci. Technol. 18 (12), 590–598.

Granier, C., Aguirrezabal, L., Chenu, K., Cookson, S.J., Dauzat, M., Hamard, P., Thioux, J., Rolland, G., Bouchier-Combaud, S., Lebaudy, A., Muller, B., Simonneau, T., Tardieu, F., 2006. PHENOPSIS, an automated platform for reproducible phenotyping of plant response to soil water deficit in *Arabidopsis thaliana* permitted the identification of an accession with low sensitivity to soil water deficit. New Phytol. 169, 623–635.

Grassini, P., Eskridge, K.M., Cassman, K.G., 2013. Distinguishing between yield advances and yield plateaus in historical crop production trends. Nat. Commun. 4, 2918.

Humplík, J.F., Lazár, D., Husičková, A., Spíchal, L., 2015. Automated phenotyping of plant shoots using imaging methods for analysis of plant stress responses – a review. Plant Methods 11, 29.

Jansen, M., Gilmer, F., Biskup, B., Nagel, K.A., Rascher, U., Fischbach, A., Briem, S., Dreissen, G., Tittmann, S., Braun, S., De Jaeger, I., Metzlaff, M., Schurr, U., Scharr, H., Walter, A., 2009. Simultaneous phenotyping of leaf growth and chlorophyll fluorescence via GROWSCREEN FLUORO allows detection of stress tolerance in *Arabidopsis thaliana* and other rosette plants. Funct. Plant Biol. 36 (11), 902–914.

Jones, H.G., Serraj, R., Loveys, B.R., Xiong, L., Wheaton, A., Price, A.H., 2009. Thermal infrared imaging of crop canopies for the remote diagnosis and quantification of plant response to water stress in the field. Funct. Plant Biol. 36, 978–989.

Kim, J.Y., Glenn, D.M., 2015. Measurement of photosynthetic response to plant water stress using a multi-modal sensing system. Trans. ASABE 58 (2), 233–240.

Konishi, A., Eguchi, A., Hosoi, F., Omasa, K., 2009. 3D monitoring spatio-temporal effects of herbicide on a whole plant using combined range of chlorophyll a fluorescence imaging. Funct. Plant Biol. 36, 874–879.

Li, L., Zhang, Q., Huang, D., 2014. A review of imaging techniques for plant phenotyping. Sensors 14, 20078–20111.

Mangus, D.L., Sharda, A., Zhang, N., 2016. Development and evaluation of thermal infrared imaging system for high spatial and temporal resolution crop water stress monitoring of corn within a greenhouse. Comput. Electron. Agric. 121, 149–159.

Meyer, G.E., Neto, J.C., 2008. Verification of color vegetation indices for automated crop imaging applications. Comput. Electron. Agric. 63, 282–293.

Mevik, B.H., Wehren, R., Liland, K.H., 2013. Pls: Partial Least Squares and Principal Component Regression.

Muñoz-Huerta, R.F., Guevara-Gonzalez, R.G., Contreras-Medina, L.M., Torres-Pacheco, I., Prado-Olivarez, J., Ocampo-Velazquez, R.V., 2013. A review of methods for sensing the nitrogen status in plants: advantages, disadvantages and recent advances. Sensors 13, 10823–10843.

Neilson, E.H., Edwards, A.M., Blomstedt, C.K., Berger, B., Moller, B.L., Gleadow, R.M., 2015. Utilization of a high-throughput shoot imaging system to examine the dynamic phenotypic responses of a C_4 cereal crop plant to nitrogen and water deficiency over time. J. Exp. Bot. 66, 1817–1832.

Norris, K.H., Barnes, R.F., Moore, J.E., Shenk, J.S., 1976. Predicting forage quality by infrared reflectance spectroscopy. J. Anim. Sci. 43, 889–897.

R Core Team, 2015. R: A Language and Environment for Statistical Computing. R Foundation for Statistical Computing, Vienna, Austria.

Romano, G., Zia, S., Spreer, W., Sanchez, C., Cairns, J., Araus, J.L., Müller, J., 2011. Use of thermography for high throughput phenotyping of tropical maize adaption in water stress. Comput. Electron. Agric. 79, 67–74.

Sankaran, S., Khot, L.R., Espinoza, C.Z., Jarolmasjed, S., Santhuvalli, V.R., Vandemark, G.J., Miklas, P.N., Carter, A.H., Pumphrey, M.O., Knowles, N.R., Pavek, M.J., 2015. Low-altitude, high-resolution aerial imaging systems for row and field crop phenotyping: a review. Eur. J. Agron. 70, 112–123.

Shenk, J.S., Workman Jr, J.J., Westerhaus, M.O., 2008. Application of NIR spectroscopy to agricultural products. In: Burns, D.A., Ciurczak, E.W. (Eds.), Handbook of Near-Infrared Analysis (3rd Edition). CRC Press, Boca Raton, FL.

Tuberrosa, R., 2012. Phenotyping for drought tolerance of crops in the genomics era. Front. Physiol. 3, 347.

Yang, W., Guo, Z., Huang, C., Duan, L., Chen, G., Jiang, N., Fang, W., Feng, H., Xie, W., Lian, X., Wang, G., Luo, Q., Zhang, Q., Liu, Q., Xiong, L., 2014. Combining high-throughput phenotyping and genome-wide association studies to reveal natural genetic variation in rice. Nat. Commun. 5, 5087.